Graphene-Covered Perovskites: An Effective Strategy to Enhance Light Absorption and Resist Moisture Degradation

Yalong Jiao[1], Fengxian Ma[1], Guoping Gao[1], Hongxia Wang[1], John Bell[1], Thomas Frauenheim[2] and Aijun Du[1,]*

[1]School of Chemistry, Physics and Mechanical Engineering Faculty, Queensland University of Technology, Garden Point Campus, QLD 4001, Brisbane, Australia

[2]Bremen Center for Computational Materials Science, University of Bremen, Am Falturm 1, 28359 Bremen, Germany

Abstract

The long-term stability of methylammonium lead triiodide ($MAPbI_3$) perovskite in moist environments is a paramount challenge to realise the commercialization of perovskite solar cells. In an attempt to address this concern, we have carried out systematic first-principles studies on the $MAPbI_3$ perovskite with hydrophobic graphene layer interfaced as water barrier. We find there is a charge transfer at graphene/$MAPbI_3$ interface and electrons can be excited from graphene into perovskite surface, leading to well separated electron-hole pair, i.e. the reduced recombination. By studying the optical property, we find the hybrid graphene/$MAPbI_3$ nanocomposite displays enhanced light absorption compared with the pristine $MAPbI_3$. Furthermore, from *ab initio* molecular dynamics simulation, the graphene/$MAPbI_3$ nanocomposite is confirmed to be able to resist the reaction with water molecule, highlighting a great advantage of this nanocomposite in promoting the long-term photovoltaic performance.

Introduction

The third-generation methylammonium lead halide perovskites $MAPbX_3$ (MA =$CH3NH^+$, X=halogen) based solar cells have undergone rapid and remarkable development over the past five years with the power conversion efficiency (PCE) improved from 3.8% [1] to a certified value of 19.3% [2] in 2014. The significant benefits of these perovskites include long charge carrier diffusion lengths, high absorption coefficients, low carrier effective masses, and compatibility with low-cost, solution-based fabrication processes.[3-5] In spite of the tremendous progress in the PCE, some great challenges[6,7] are still urgent to be addressed toward the worldwide commercialization. One of the most crucial concerns for perovskites is the lack of long-term stability [8] under water exposure. In other words, rapid degradation in moist environments has suggested that water may corrode perovskites, which would inevitably limit its outdoor applications. Therefore, how to prevent chemical reaction between water and perovskite surface is vital for the industrial applications.

Graphene as a two-dimensional one-atom thick sheet of carbon has attracted enormous interest due to its unique properties and a wide variety of potential applications including photodetectors[9] and solar cells[10]. Graphene has demonstrated exceptional thermal and chemical stability[11] under various circumstances. It also possesses excellent optical properties with 97.7% optical transparency, so graphene coatings[12] is not expected to degrade the light absorption ability of the underlying materials. Additionally, the unique properties of hydrophobic graphene will enable it to be an excellent barrier for protecting solar cell materials from unwanted chemical reactions.

Most recently, great experimental efforts have been carried out on the synthesis of hybrid graphene/$MAPbI_3$ nanocomposites[13], in which enhanced photovoltaic properties have been demonstrated. However, the underlying mechanism and the stability in humid environment remain wholly unclear. In this work, first-principle calculations are performed to study the nature of interface between hydrophobic

graphene and $MAPbI_3$. Two different terminations, namely MAI-terminated (001) and PbI_2-terminated (001) surfaces for the tetragonal phase of perovskite $CH_3NH_3PbI_3$ are considered. We first examine the origin of charge transfer at the graphene/$MAPbI_3$ interface. Then the electronic and optical properties of graphene/$MAPbI_3$ nanocomposite were investigated. Lastly, *ab initio* molecular dynamics (AIMD) simulations are performed to prove the stabilities of graphene/$MAPbI_3$ systems under water exposure.

Computational Methods

All the calculations were performed based on density functional theory (DFT) by using the plane wave basis Vienna Ab initio simulation package (VASP) code,[14,15] implementing the projector augment wave (PAW) method. [16] The generalized gradient approximation in the Perdew, Burke, and Ernzerhof form (GGA-PBE) [17] was used as exchange correlation functional for the calculations of geometries, electronic and optical properties of graphene/$MAPbI_3$ system. A damped van der Waals correction was incorporated using Grimme's scheme[18] to better describe the non-bonding interaction. Notice that the spin-orbital-coupling (SOC) effect was not taken into consideration in the current calculations because the electrical properties could be well described at PBE level compared with experiments, although it was somewhat fortuitous, i.e., the accidental cancellation of the underestimation by GGA-PBE method[19]. The vacuum space perpendicular to the MAI (001) and PbI_2 (001) surface was more than 20 Å, which was enough to avoid the interaction between neighboring slabs. Monkhorst−Pack k-points [20] of 4 x 2x 1 and 8 x 4x 1 points were used to sample the Brillouin zone for geometry optimization and calculating density of states, respectively. The cut-off energies for plane waves were set to be 500 eV, and the residual force and energy on each atom during structure relaxation were converged to 0.008 eV/Å and 10^{-5}eV, respectively. To understand the mechanism of the interface charge transfer in the hybrid graphene/$MAPbI_3$ system, work functions of the

graphene layer, bare MAI-terminated (001) and PbI_2-terminated (001) surfaces were calculated via aligning the Fermi level relative to the vacuum energy level.

A rectangle 2 x 7 graphene layer (a=4.26, b=2.46, 56 carbon atoms) was used to match a 1 x2 x 2 four atomic layer MAPbI3 (a=b=8.74, c=12.92, from GGA-PBE calculation) surface slab containing 16 Pb, 48 I, 16 C, 16 N and 96 H atoms with three bottom layers fixed at bulk position in a supercell. The whole system contained totally 248 atoms with 864 valence electrons and the lattice mismatch was approximately 1%.

AIMD simulations have been undertaken to study the stability of Hybrid Graphene/$MaPbI_3$ systems in water environment. The $MaPbI_3$ slab was sandwiched by two layers of graphene as the water barriers and 36 water molecules were placed on the top of graphene layer. The whole system contained 400 atoms with 1304 valence electrons for MAI surface slab and 382 atoms with 1304 valence electrons for PbI_2 surface slab. Only Γ-point was used for the Brillouin zone sampling and the energy cut-off was 300 eV. During the AIMD simulation, the systems were heated up and maintained at the temperature of 300 K for 6.0 ps in a NVT (canonical) ensemble with a time step of 1 fs.

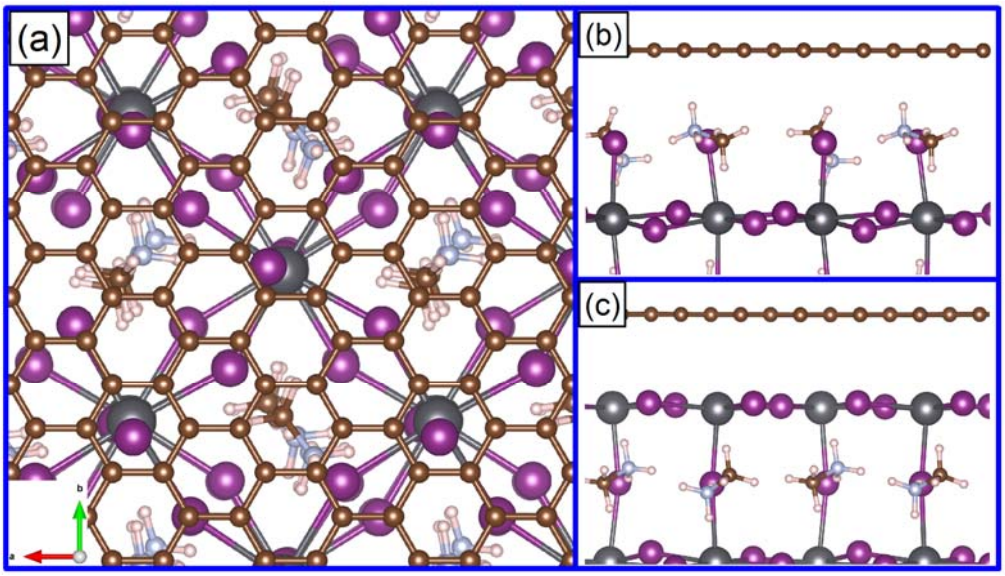

Figure 1 (a) The top view and (b) side view of the optimized graphene/MAI interface; (c) side view of the graphene/PbI_2 interface. Brown, black, silver, violet and light pink balls represent C, Pb, N, I and H atoms, respectively.

Figure 1 presents the top view of the graphene/$CH_3NH_3PbI_3$ interface model used in our calculations. The equilibrium distance between the graphene layer and the MAI/PbI_2 surface slab is 2.8/3.8 Å. The interface binding energy was obtained according to the following equation

$$E_b = E_{comb} - E_{gra} - E_I$$

where E_{comb}, $E_{graphene}$ and E_I are the total energy of the relaxed hybrid graphene/$MAPbI_3$ complex, pure graphene sheet and $MAPbI_3$ slab, respectively. The interface binding energy is -1.52 eV for hybrid graphene/MAI surface and -1.79 eV for graphene/PbI_2 complex, which indicates very high structural stability.

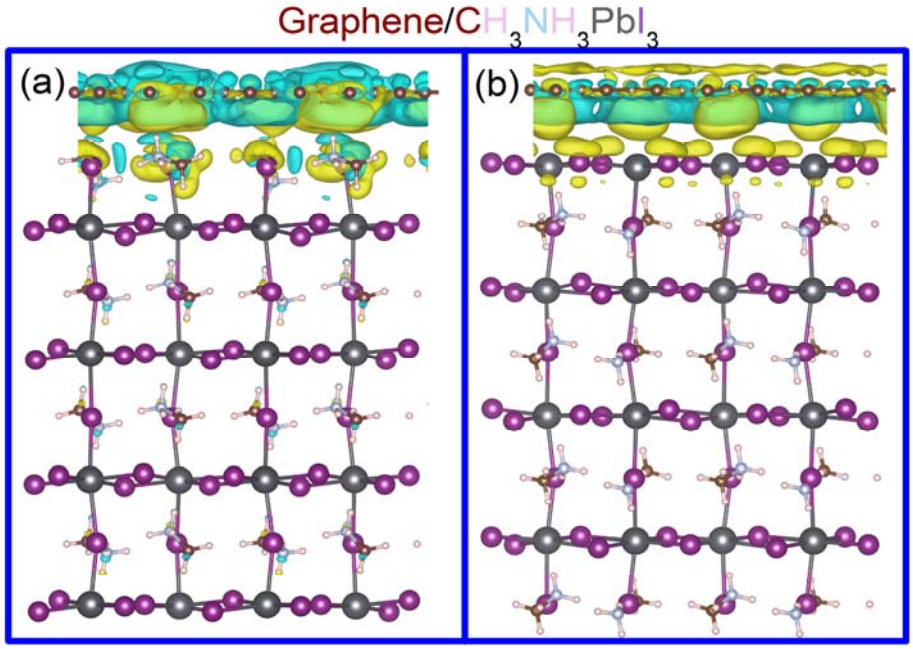

Figure 2 The side view of 3D charge density difference plot for the interface between a graphene sheet and a 4-layer (a) MAI and (b) PbI_2 surface slab. Yellow and cyan isosurfaces represent electron accumulation and depletion in the 3D space with an isovalue of 0.001 e/Å3.

To characterize the electron coupling at the graphene/$MAPbI_3$ interface, 3D charge density difference are plotted by subtracting electronic charge of hybrid graphene/$MAPbI_3$ nanocomposite from pure graphene layer and separated MAI or PbI_2 surface slab as shown in Fig. 2a and 2b, respectively. For graphene/MAI system, it can be seen that at the equilibrium, charge will redistribute within graphene layer and,

all iodine atoms in MAI surface show significant electron accumulation, while all charge depletion occurs around CH_3NH_3 molecules. For graphene/PbI_2 system, charge transfer from the graphene layer to the first layer of PbI_2 surface in the ground electronic state can be obviously seen. The dominating charge transfer derives between graphene and iodine atoms at PbI_2 surface, and this is able to induce efficient hole accumulation in the graphene layer and electron accumulation at perovskite surface, leading to the enhanced electrical conductivity in the $MAPbI_3$ nanosheet. Therefore the electron-hole pairs can be well separated with each other.

To understand the origin of such an interface charge-transfer in the hybrid grpahene/$MAPbI_3$ complex, work functions for the graphene layer, MAI and PbI_2 surface slabs were calculated by aligning the Fermi level relative to the vacuum energy level (Fig. S1 in the Supporting Information). The work functions for graphene were found to be 4.29, which is closed to the experimental measurements[21] and the values for MAI and PbI_2 surfaces are 4.60 and 4.75 eV, respectively. The spontaneous interfacial charge transfer from graphene to $MAPbI_3$ can be simply rationalized in terms of the higher work functions on MAI and PbI_2 surfaces which usually act as "electron acceptor".

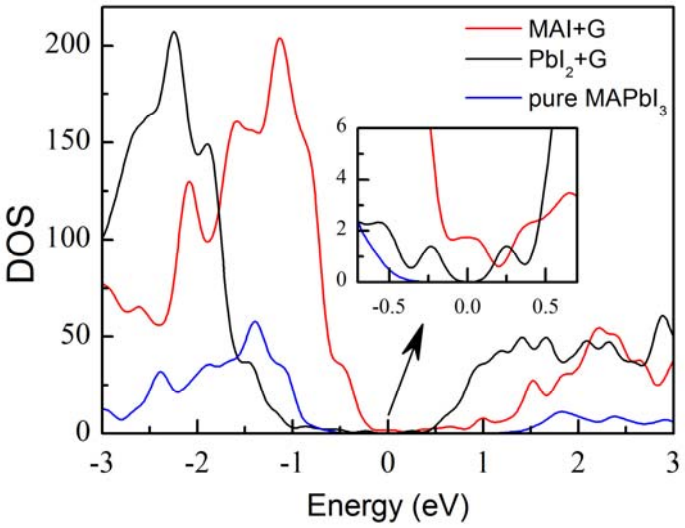

Figure 3 Total-DOS plots for free-standing (blue line) $MaPbI_3$, graphene/MAI(001) surface (red line) and graphene/PbI_2 (001) surface (black line). The Fermi level was set to zero.

To study the electronic properties of the hybrid system, we plot the total density of states (TDOS) for free-standing $MaPbI_3$, graphene/MAI (001) and graphene/PbI_2 (001) surface as shown in Fig. 3. For graphene/MAI(001) nanocomposite, the Fermi level show downwards shift by around 0.2 eV relative to the Dirac point, while the Dirac point for graphene/PbI_2 system remains nearly unchanged. This may due to the fact that the interlayer distance for graphene/MAI (2.8 Å) is much shorter, which would display much stronger interface interaction compared with that in graphene/PbI_2. From the projected density of state (PDOS, see Fig. S2a and S2b), we find the strong hybridizations of *p*-orbital of Pb, *p*-orbital of I and *p*-orbital of C (graphene) in the vicinity of the Fermi level, which is mainly due to the high binding energy between graphene and MAI surface. For PbI_2 surface (Fig. S3b), by contrast, the band edges of Pb and I display obvious downwards shift about 1 eV and it is clearly visible that graphene layer plays a significant role in state accumulation at interface near Fermi level (the inset of Fig. S3b). It should be noted that the inhomogeneous hybrid system induces charge redistribution in layers, forming interlayer electron-hole puddles, which may significantly enhance the electron conductivity as well as generate new photovoltaic and catalytic activities. Furthermore, the new introduced states from graphene near Fermi level are expected to enhance the conductance in this hybrid system.

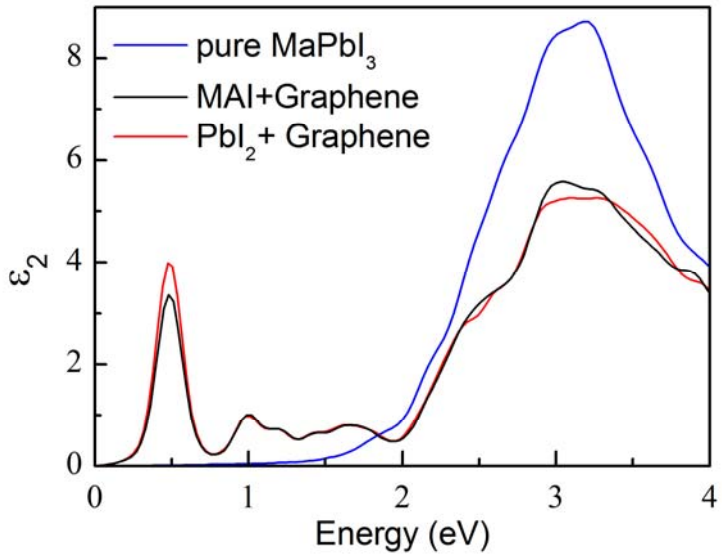

Figure 4 The imaginary part of the dielectric function of pristine $MAPbI_3$ (blue line), the hybrid graphene/MAI (001) nanocompoiste (red line) and the hybrid graphene/PbI_2 (001) nanocompoiste for the polarization vector perpendicular to the surface

Previous studies[22,23] have revealed that the charge-transfer complex is able to improve photocatalytic activities under light illumination. The similar behaviour is also found in current hybrid graphene /$MAPbI_3$ systems as shown in Fig. 4. The imaginary part of the dielectric function for $MAPbI_3$ bulk and a hybrid graphene/$MAPbI_3$ were calculated. As GGA-PBE calculation can yield good results of band gap for $MaPbI_3$, we believe the absorption edge of the systems can be well-predicted at this level. It can be seen clearly from the calculated imaginary part of the dielectric function, the red shift of absorption edge is as large as 1.5 eV for the hybrid graphene/MAI and graphene/PbI_2 nanocomposite compared to that for the pristine $MAPbI_3$, demonstrating more effective Infrared (IR) light absorption and enhanced visible light response. The onsets of optical absorption for hybrid graphene/$MAPbI_3$ lie in the IR light region, which is attributed to the electronic structure of the hybrid systems. According to the PDOS of graphene/PbI_2 system, the VBM is totally dominated by *2p* orbital of C (C-*2p*) from graphene while the CBM is mainly contributed by C-*2p* from graphene and marginally from Pb-*6p*. Whereas, the transition from occupied C-*2p* state to unoccupied C-*2p* orbital is symmetrically forbidden. Only the transition from C-*2p* to Pb-*6p* is allowed. By contrast for Graphene/MAI system, absorption peak in low-energy region mainly derives from the transition between C-*2p* from graphene and I-*5p*. Clearly, graphene plays an important role in the enhancement of light response and the hybrid graphene/$MAPbI_3$ nanocomposite is expected to display the enhanced photocatalytic activities under the light irradiation.

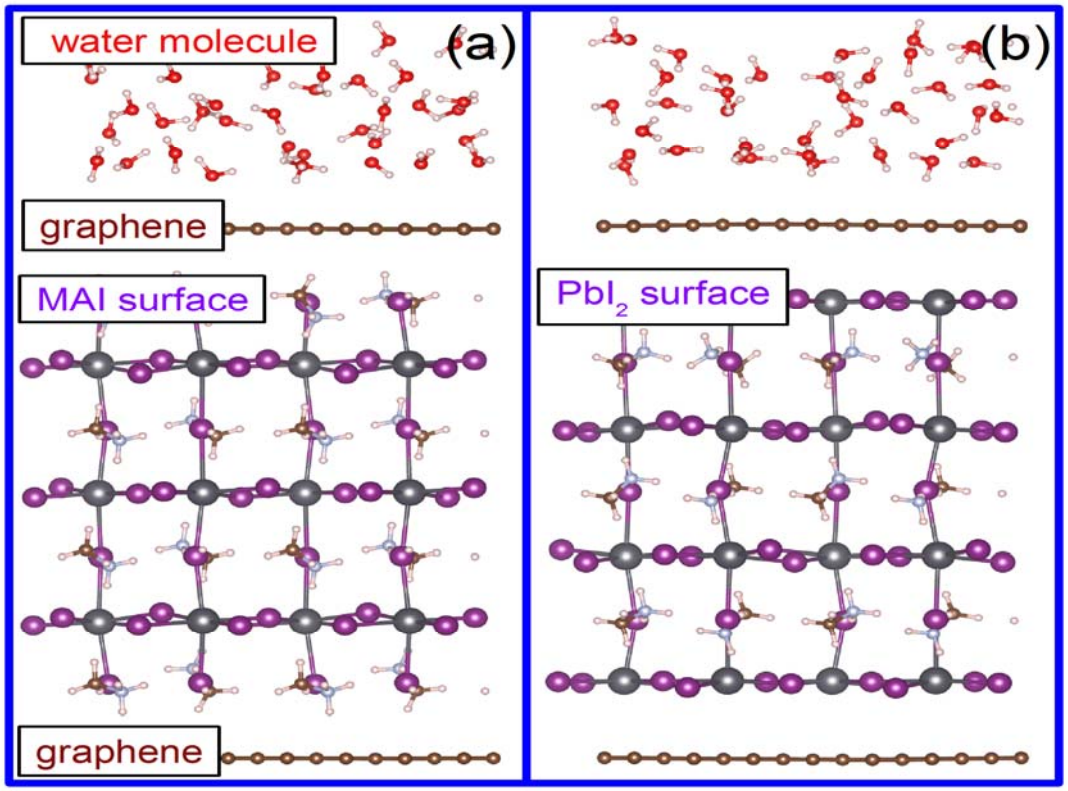

Figure 5 The relaxed structures of water adsorbing on graphene-coated (a) MAI-terminated and (b) PbI_2-terminated surfaces

Having confirmed the excellent optical properties of graphene/$MAPbI_3$ nanocomposite, then we turn to estimate their stabilities surrounded by water molecules. The relaxed structures of water adsorbing on the neutral graphene-covered MAI and PbI_2 surfaces are shown in Fig. 5a and 5b, respectively. In these two cases, 36 water molecules are contained in the supercell and the water density is close to the density at room temperature and 1atm pressure. First the geometries was fully relaxed at 0 K and the minimum distances between hydrogen atoms in water and graphene layers $d_{h\text{-}g}$ for the two cases were calculated to be 2.16 and 2.24 Å, respectively. During the AIMD simulation, the distance $d_{h\text{-}g}$ and $d_{g\text{-}m}$ did not alter significantly and no water molecule was able to reach the perovskite surface and bond with Pb cations (see movie files in the supporting information). Therefore, the graphene-coated strategy can effectively protect $MAPbI_3$ from the reaction with water, thus maintaining the long-term stability of $MaPbI_3$ in the moist environment and enhancing visible and infrared light response.

Conclusion

In summary, we have studied the electronic, optical properties and long-term stability under water exposure in the hybrid graphene/$MAPbI_3$ nanocomposites. The high interface binding energy indicates very high structural stability and the calculated imaginary part of the dielectric function demonstrates the enhanced light absorption compared with the pristine $MAPbI_3$. Furthermore, the electrons and holes can be well separated due to the charge transfer at the graphene/MAPbI3 interface, leading the reduction of electron−hole recombination. Most importantly, we also confirm that the stability of methylammonium lead triiodide in water environment can be maintained via the graphene-coated strategy. Our results offer new theoretical insights and are expected to stimulate new experiments along this direction by fabricating the long-term stable perovskite solar cells in laboratory.

Acknowledgements:

We acknowledge generous grants of high-performance computer time from computing facility at Queensland University of Technology and Australian National Facility. A.D. greatly appreciates the Australian Research Council QEII Fellowship and financial support of the Australian Research Council under Discovery Project (DP130102420). T. F. and A. D. also acknowledge the financial support (for exchange and visiting) by DAAD/PPPATN57058295.

Supporting Information

Average electrostatic potentials for graphene, bare MAI-terminated and PbI_2-terminated surface; Movies during AIMD simulations for MAI-terminated and PbI_2-terminated surface.

Reference

(1) Kojima, A.; Teshima, K.; Shirai, Y.; Miyasaka, T. Organometal Halide Perovskites as Visible-Light Sensitizers for Photovoltaic Cells. *J. Am. Chem. Soc.* **2009**, *131*, 6050-6051.

(2) Zhou, H.; Chen, Q.; Li, G.; Luo, S.; Song, T.-b.; Duan, H.-S.; Hong, Z.; You, J.; Liu, Y.; Yang, Y. Interface engineering of highly efficient perovskite solar cells. *Science* **2014**, *345*, 542-546.

(3) Xing, G.; Mathews, N.; Sun, S.; Lim, S. S.; Lam, Y. M.; Grätzel, M.; Mhaisalkar, S.; Sum, T. C. Long-Range Balanced Electron- and Hole-Transport Lengths in Organic-Inorganic CH3NH3PbI3. *Science* **2013**, *342*, 344-347.

(4) Ponseca, C. S.; Savenije, T. J.; Abdellah, M.; Zheng, K.; Yartsev, A.; Pascher, T.; Harlang, T.; Chabera, P.; Pullerits, T.; Stepanov, A.; Wolf, J.-P.; Sundström, V. Organometal Halide Perovskite Solar Cell Materials Rationalized: Ultrafast Charge Generation, High and Microsecond-Long Balanced Mobilities, and Slow Recombination. *J. Am. Chem. Soc.* **2014**, *136*, 5189-5192.

(5) Stoumpos, C. C.; Malliakas, C. D.; Kanatzidis, M. G. Semiconducting Tin and Lead Iodide Perovskites with Organic Cations: Phase Transitions, High Mobilities, and Near-Infrared Photoluminescent Properties. *Inorganic Chemistry* **2013**, *52*, 9019-9038.

(6) Yang, J.; Siempelkamp, B. D.; Liu, D.; Kelly, T. L. Investigation of CH3NH3PbI3 Degradation Rates and Mechanisms in Controlled Humidity Environments Using in Situ Techniques. *ACS Nano* **2015**, *9*, 1955-1963.

(7) Boix, P. P.; Nonomura, K.; Mathews, N.; Mhaisalkar, S. G. Current progress and future perspectives for organic/inorganic perovskite solar cells. *Materials Today* **2014**, *17*, 16-23.

(8) Noh, J. H.; Im, S. H.; Heo, J. H.; Mandal, T. N.; Seok, S. I. Chemical Management for Colorful, Efficient, and Stable Inorganic–Organic Hybrid Nanostructured Solar Cells. *Nano Lett.* **2013**, *13*, 1764-1769.

(9) Freitag, M.; Low, T.; Xia, F.; Avouris, P. Photoconductivity of biased graphene. *Nat. Photonics* **2013**, *7*, 53-59.

(10) Mueller, T.; Xia, F.; Avouris, P. Graphene photodetectors for high-speed optical communications. *Nat. Photonics* **2010**, *4*, 297-301.

(11) Liu, L.; Ryu, S.; Tomasik, M. R.; Stolyarova, E.; Jung, N.; Hybertsen, M. S.; Steigerwald, M. L.; Brus, L. E.; Flynn, G. W. Graphene Oxidation: Thickness-Dependent Etching and Strong Chemical Doping. *Nano Lett.* **2008**, *8*, 1965-1970.

(12) Prasai, D.; Tuberquia, J. C.; Harl, R. R.; Jennings, G. K.; Bolotin, K. I. Graphene: Corrosion-Inhibiting Coating. *ACS Nano* **2012**, *6*, 1102-1108.

(13) Lee, Y.; Kwon, J.; Hwang, E.; Ra, C.-H.; Yoo, W. J.; Ahn, J.-H.; Park, J. H.; Cho, J. H. High-Performance Perovskite–Graphene Hybrid Photodetector. *Adv. Mater.* **2015**, *27*, 41-46.

(14) Kresse, G.; Furthmüller, J. Efficiency of ab-initio total energy calculations for metals and semiconductors using a plane-wave basis set. *Comput. Mater. Sci.* **1996**, *6*, 15-50.

(15) Kresse, G.; Furthmüller, J. Efficient iterative schemes for ab initio total-energy calculations using a plane-wave basis set. *Phys. Rev. B* **1996**, *54*, 11169-11186.

(16) Blöchl, P. E. Projector augmented-wave method. *Phys. Rev. B* **1994**, *50*, 17953-17979.

(17) Perdew, J. P.; Burke, K.; Ernzerhof, M. Generalized Gradient Approximation Made Simple. *Phys. Rev. Lett.* **1996**, *77*, 3865-3868.

(18) Grimme, S. Semiempirical GGA-type density functional constructed with a long-range dispersion correction. *J. Comput. Chem.* **2006**, *27*, 1787-1799.

(19) Mosconi, E.; Amat, A.; Nazeeruddin, M. K.; Grätzel, M.; De Angelis, F. First-Principles Modeling of Mixed Halide Organometal Perovskites for Photovoltaic Applications. *J. Phys. Chem. C* **2013**, *117*, 13902-13913.

(20) Monkhorst, H. J.; Pack, J. D. Special points for Brillouin-zone integrations. *Phys. Rev. B* **1976**, *13*, 5188-5192.

(21) Yu, Y.-J.; Zhao, Y.; Ryu, S.; Brus, L. E.; Kim, K. S.; Kim, P. Tuning the Graphene Work Function by Electric Field Effect. *Nano Lett.* **2009**, *9*, 3430-3434.

(22) Du, A.; Smith, S. C. Electronic Functionality in Graphene-Based Nanoarchitectures: Discovery and Design via First-Principles Modeling. *J. Phys. Chem. Lett.* **2011**, *2*, 73-80.

(23) Park, Y.; Singh, N. J.; Kim, K. S.; Tachikawa, T.; Majima, T.; Choi, W. Fullerol–Titania Charge-Transfer-Mediated Photocatalysis Working under Visible Light. *Chemistry – A European Journal* **2009**, *15*, 10843-10850.